In Situ Elucidation of the Active State of Co−CeO$_x$ Catalysts in the Dry Reforming of Methane: The Important Role of the Reducible Oxide Support and Interactions with Cobalt

Feng Zhang,[†] Zongyuan Liu,[‡] Shuhao Zhang,[†] Nusnin Akter,[†] Robert M. Palomino,[‡] Dimitriy Vovchok,[§] Ivan Orozco,[§] David Salazar,[‡] José A. Rodriguez,[‡,§] Jordi Llorca,[∥] Jaeha Lee,[⊥] DoHeui Kim,[⊥] Wenqian Xu,[#] Anatoly I. Frenkel,[†,‡] Yuanyuan Li,[†] Taejin Kim,*[,†] and Sanjaya D. Senanayake*[,‡]

[†]Materials Science and Chemical Engineering Department and [§]Chemistry Department, Stony Brook University, Stony Brook, New York 11794 United States

[‡]Chemistry Department, Brookhaven National Laboratory, Upton, New York 11973 United States

[∥]Institute of Energy Technologies, Department of Chemical Engineering and Barcelona Research Center in Multiscale Science and Engineering, Technical University of Catalonia, 08019 Barcelona, Spain

[⊥]School of Chemical and Biological Engineering, Institute of Chemical Processes, Seoul National University, Seoul 151-744, Republic of Korea

[#]X-ray Science Division, Advanced Photon Source, Argonne National Laboratory, Argonne, Illinois 60439, United States

S *Supporting Information*

ABSTRACT: The activation of methane and its dry reforming with CO$_2$ was systematically studied over a series (2−30 wt %) of Co (∼5 nm in size) loaded CeO$_2$ catalysts, with an effort to elucidate the interplay between Co and CeO$_2$ during the catalytic process using in situ methods. The results of in situ time-resolved X-ray diffraction (TR-XRD) show a strong interaction of methane with the CoO$_x$−CeO$_2$ systems at temperatures between 200 and 350 °C. The hydrogen produced by the dissociation of C−H bonds in methane leads to a full reduction of Co oxide, Co$_3$O$_4$ → CoO → Co, and a partial reduction of ceria with the formation of some Ce^{3+}. Upon the addition of CO$_2$, a catalytic cycle for dry reforming of methane (DRM) was achieved on the CoO$_x$−CeO$_2$ powder catalysts at temperatures below 500 °C. A 10 wt % Co−CeO$_2$ catalyst was found to possess the best catalytic activity

among various cobalt loading catalysts, and it exhibits a desirable stability for the DRM with a minimal effect of carbon accumulation. The phase transitions and the nature of active components in the catalyst were investigated under reaction conditions by in situ time-resolved XRD and ambient-pressure X-ray photoelectron spectroscopy (AP-XPS). These studies showed dynamic evolutions in the chemical composition of the catalysts under reaction conditions. CO$_2$ attenuated the reducing effects of methane. Under optimum CO- and H$_2$-producing conditions, both XRD and AP-XPS indicated that the active phase involved a majority of metallic Co with a small amount of CoO, both supported on a partially reduced ceria (Ce^{3+}/Ce^{4+}). We identified the importance of dispersing Co, anchoring it onto the ceria surface sites, and then utilizing the redox properties of CeO$_2$ for activating and then oxidatively converting methane while inhibiting coke formation. Furthermore, a synergistic effect between cobalt and ceria and likely the interfacial sitee are essential to successfully close the catalytic cycle.

KEYWORDS: *cobalt, ceria, in situ XRD, AP-XPS, methane dry reforming*
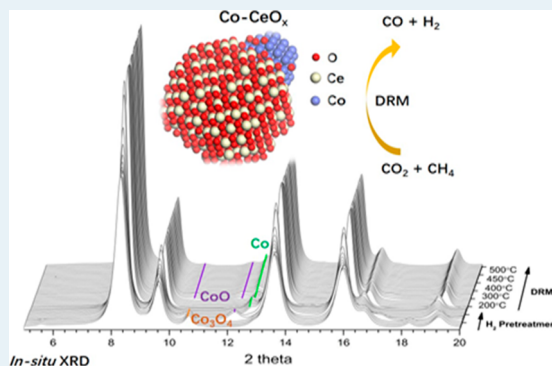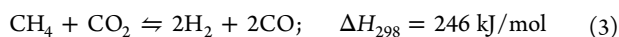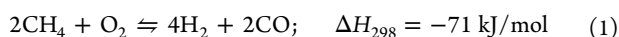
■ INTRODUCTION

Natural gas and biogas are both methane-enriched gases and have become cheap, abundant alternatives to traditional fossil fuels such as petroleum and coal.[1−3] In addition to being combusted with O$_2$ as a source in the production of electricity or heat, natural gas and biogas can be used more efficiently as chemical feedstock in the manufacture of commodity chemicals, and this can be achieved by reforming CH$_4$ to syngas (H$_2$ and CO) and subsequently converting syngas to upgraded chemicals.[4,5] There are three oxidative pathways to produce syngas from methane: (1) partial oxidation, (2) steam reforming and (3) dry reforming:

$$2CH_4 + O_2 \leftrightharpoons 4H_2 + 2CO; \quad \Delta H_{298} = -71 \text{ kJ/mol} \quad (1)$$

$$CH_4 + H_2O \leftrightharpoons 3H_2 + CO; \quad \Delta H_{298} = 206 \text{ kJ/mol} \quad (2)$$

$$CH_4 + CO_2 \leftrightharpoons 2H_2 + 2CO; \quad \Delta H_{298} = 246 \text{ kJ/mol} \quad (3)$$

The dry reforming of methane (DRM) is the most difficult of these processes, but it is desirable as an initial step in the Fischer–Tropsch (F–T) process and methanol synthesis, owing to its 1:1 production ratio of CO and H_2.[6−9] It utilizes a CH_4 and CO_2 mixture which simplifies the separation process of both natural gas and biogas.[10−12] Moreover, both methane and CO_2 are active greenhouse gases, and the exploitation of them during the DRM reaction could potentially mitigate global warming and climate change.[13−16] From a fundamental perspective, in the DRM process, CO_2 offers a poor source of O to the C−H bond activation process, on account of large activation barriers to extract O from CO_2 unlike the case of O_2 and H_2O.[17] As a result, the DRM reaction involves a soft oxidative activation during the conversion of CH_4. Since the interaction with CH_4 and CO_2 can change the chemical state of a catalyst, a detailed study of the DRM process using in situ techniques can lead to a fundamental understanding on how to activate CH_4 selectively by avoiding pathways to complete oxidation, hence benchmarking catalyst behavior under difficult reaction conditions.

Typically, noble metals (e.g., Rh, Ru, Pd, Ir, and Pt) possess good activity and coke resistance for this reaction, but they are susceptible to rapid deactivation at elevated reaction temperature by particle sintering or poor dispersion, in addition to their high cost and low abundance.[18−22] The cheaper and more earth-abundant metals (e.g., Ni, Co, and Fe) are an alternative option. The addition of Co to Ni-based catalysts leads to enhanced stability and resistance to coke formation owing to the Co oxophilicity.[6,23−30] It was proposed that the presence of O on Co leads to a more feasible pathway for CO_2-mediated activation of CH_4, and the mechanism is highly dependent on the enhanced oxophilicity that is unique to Co.[26] This aspect is particularly complex to follow when Co is coupled to ceria, a reducible oxide support well-known for its ability to transfer oxygen readily.

Although several models or hypotheses have been proposed to explain the performance of Co-based catalysts for the DRM reaction, the catalysts' structural and chemical state evolution during the reaction has not been investigated in great detail.[24,31] Our recent studies of DRM reactions over a model system generated by depositing Co atoms on a well-defined planar $CeO_2(111)$ surface show activation of methane at room temperature.[32] Cooperative effects between the Co and oxygen sites of ceria make possible the bonding of methane and the activation of the C−H bond at low temperature.[32] The CH_x deposited on the surface can undergo further transformation in DRM reactions or be used as the starting point for the production of valuable chemicals.[32] In this paper, we move from a $CoO_x–CeO_2(111)$ model catalyst into cobalt−ceria powders which can be used in technical applications. In these powder systems, it is important to study the nature of the interactions between cobalt and ceria and determine how they affect the activation of methane. In the case of $CoO_x–CeO_2$ (111), one has a nonexpensive system which can perform DRM reactions and does not undergo deactivation due to coke deposition.[32]

In this work, we synthesized a series of ceria-supported powder catalysts with various cobalt loadings (2−30 wt %). In situ time-resolved X-ray diffraction (TR-XRD) was used to study the interaction of methane with these $CoO_x–CeO_2$ systems, and a massive reduction of these oxide systems was observed at temperatures between 200 and 350 °C. The hydrogen produced by the dissociation of C−H bonds in methane leads to a full reduction of Co and a partial reduction of ceria. For the DRM process, a catalytic cycle was achieved on the $CoO_x–CeO_2$ powder catalysts below 500 °C. The behavior of these systems under reaction conditions was investigated using a combination of in situ TR-XRD and ambient-pressure X-ray photoelectron spectroscopy (AP-XPS). Our studies show a dynamic evolution in the chemical composition of the catalysts and highlight the importance of metal−oxide interactions for the activation of methane on powder cobalt−ceria catalysts.

■ EXPERIMENTAL SECTION

Synthesis of Co−CeO₂ Catalysts. An incipient wetness impregnation method was used to prepare a series of Co−CeO_2 catalysts with different Co loadings (2, 4, 6, 8, 10, 20, and 30 wt %). The intended amount of cobalt(II) nitrate hexahydrate ($Co(NO_3)_2·6H_2O$, ACS grade, 98.0−102.0%, manufactured by Alfa Aesar) was first dissolved in deionized water at room temperature, and the solution was dropwise added to cerium oxide (CeO_2, HAS 5, manufactured by Rhodia) for impregnation. The mixed slurries were then aged at room temperature for 12 h and dried overnight at 120 °C. The resulting products were finally calcined at 400 °C (5 °C/min) for 6 h with 100 mL/min compress airflow in a tubular furnace (Lindberg/Blue Mini-Mite Tube Furnace, Model TF55030A-1). The synthesized $CoO_x–CeO_2$ catalysts were crushed and sieved to 425 μm size before additional testing.

Catalyst Characterization. N_2 adsorption/desorption isotherms were measured on a Micromeritics ASAP 2010 apparatus at a liquid N_2 temperature of −196 °C. Before analysis, 0.1 g of catalyst was pretreated at 300 °C for 4 h under evacuation conditions. The specific surface area was calculated by using the Brunauer−Emmett−Teller (BET) method.

Scanning transmission electron microscope (STEM) and high-resolution transmission electron microscope (HRTEM) images were taken for 10 and 30 wt % Co−CeO_2 as-prepared catalysts and for 8 wt % Co−CeO_2 post-experiment catalysts. Samples were dispersed in an ethanol suspension, and a drop of the suspension was placed over a grid with holey-carbon film. The microscope used for STEM and HRTEM was a FEI Tecnai F20 equipped with a field emission electron gun operating at 200 kV. The ex situ XRD characterization and the in situ H_2-TPR (temperature-programmed reduction), CH_4-TPR, and DRM XRD measurements for the 10 wt % Co−CeO_2 catalyst were performed at beamline 17BM ($\lambda = 0.45260$ Å) at the Advanced Photon Source (APS) with a Clausen cell flow reactor.[33] 10 cc/min H_2 and 10 cc/min CH_4 were used for H_2-TPR and CH_4-TPR, respectively, and the sample was heated from room temperature to 700 °C with a 2 °C/min ramping rate. For the DRM reaction, a 10 cc/min flow rate of pure H_2 was first used to pretreat the catalyst at 550 °C for 1 h. The gas line was subsequently purged by He at room temperature before introduction of a 10 cc/min flow of a gas mixture containing 20% CO_2, 20% CH_4, and 60% He for a 1:1 CO_2/CH_4 molar ratio. The samples were stepwise heated to 500 °C with a 10 °C/min ramping rate. An in-line residual gas analyzer was used to track the evolution of the gaseous species right after the flow cell. Two-dimensional XRD images were

collected continuously with a Perkin Elmer, a Si flat panel detector through the reaction processes. The XRD data were subsequently processed with GSAS-II to obtain diagrams of Intensity versus 2θ, and Rietveld analyses were also performed through GSAS-II.[34] The ex situ X-ray absorption near edge structure (XANES) measurements of 10 wt % Co−CeO$_2$ catalyst were performed at beamline BL 2−2 at the Stanford Synchrotron Radiation Light source (SSRL), SLAC National Accelerator Laboratory. The Co K edge data were collected in fluorescence yield mode using a 13-channel Ge detector.

Catalytic Activity Test. A series of activity tests were carried out on various cobalt-loading samples for the DRM reaction. The powder catalysts were loaded into a silica capillary reactor (0.9 mm i.d., 1.1 mm o.d.) and mounted on a flow system. The reaction conditions were the same as described above for the in situ XRD DRM test, and the catalytic activity of different cobalt-loading samples was measured through mass spectrometer and gas chromatography devices. In addition, CH$_4$-TPR was also performed on 10 wt % Co−CeO$_2$ catalysts, plain CeO$_2$, plain Co$_3$O$_4$, and a physical mixture of CeO$_2$ and Co$_3$O$_4$ to compare the methane activation of these samples and investigate possible metal−support interactions. The catalysts were heated to 700 °C with a 10 °C/min ramping under pure CH$_4$, and the effluent gas was monitored by a mass spectrometer.

AP-XPS. A commercial SPECS AP-XPS chamber equipped with a PHOIBOS 150 EP MCD-9 analyzer at the Chemistry Division of Brookhaven National Laboratory (BNL) was used for XPS analysis (resolution: ∼0.4 eV). The Ce 3d photoemission line with the strongest Ce^{4+} feature (916.9 eV) was used for the energy calibration. The powder sample (10 wt % Co−CeO$_2$ catalyst) was pressed on an aluminum plate and then loaded into the AP-XPS chamber. A 10 mTorr sample of H$_2$ was used to pretreat the sample at 550 °C for 1 h before a reaction mixture of 75 mTorr of CH$_4$ and 75 mTorr of CO$_2$ was introduced into the reaction chamber through a high precision leak valve. O 1s, Ce 4d, Co 2p, and Ce 3d XPS regions were collected at room temperature, 400 and 500 °C, under the reaction gas environment.

■ RESULTS

Characterization of the As-Prepared CoO$_x$−CeO$_2$ Catalysts. Figure 1a shows the XRD patterns of the prepared 10 wt % Co−CeO$_2$ sample with bulk CeO$_2$ and Co$_3$O$_4$ standards for comparison. There are only two phases detected in the prepared Co−CeO$_2$ sample. The majority of the diffraction peaks come from the fluorite structure of CeO$_2$, and the peaks at 5.58°, 10.70°, 16.80°, and 18.31° correspond to the (111), (311), (333), and (440) planes of Co$_3$O$_4$, respectively.[35] XRD patterns for catalysts with various cobalt loadings are provided in Figure S1. The spinel Co$_3$O$_4$ characteristic peaks can be observed starting from 4 wt % Co−CeO$_2$ catalyst with a gain in the intensity of the peaks as metal loadings were increased to 30 wt %. The absence of these characteristic peaks of Co$_3$O$_4$ in 2 wt % catalysts is due to the poor crystallinity of cobalt at such low loading, which is hard to capture by XRD (Figure S1 and Table S1), while the sharp Co$_3$O$_4$ peaks in 30 wt % catalyst indicate much larger average crystallite size of the Co oxide phase, implying the agglomeration of the Co$_3$O$_4$ during the synthesis process. From the GSAS-II refinement results (Table S1), one can see that CeO$_2$ particles in Co−CeO$_2$ catalysts are around 6−7 nm, and the BET data in Table S1 show that the surface areas of the samples continually
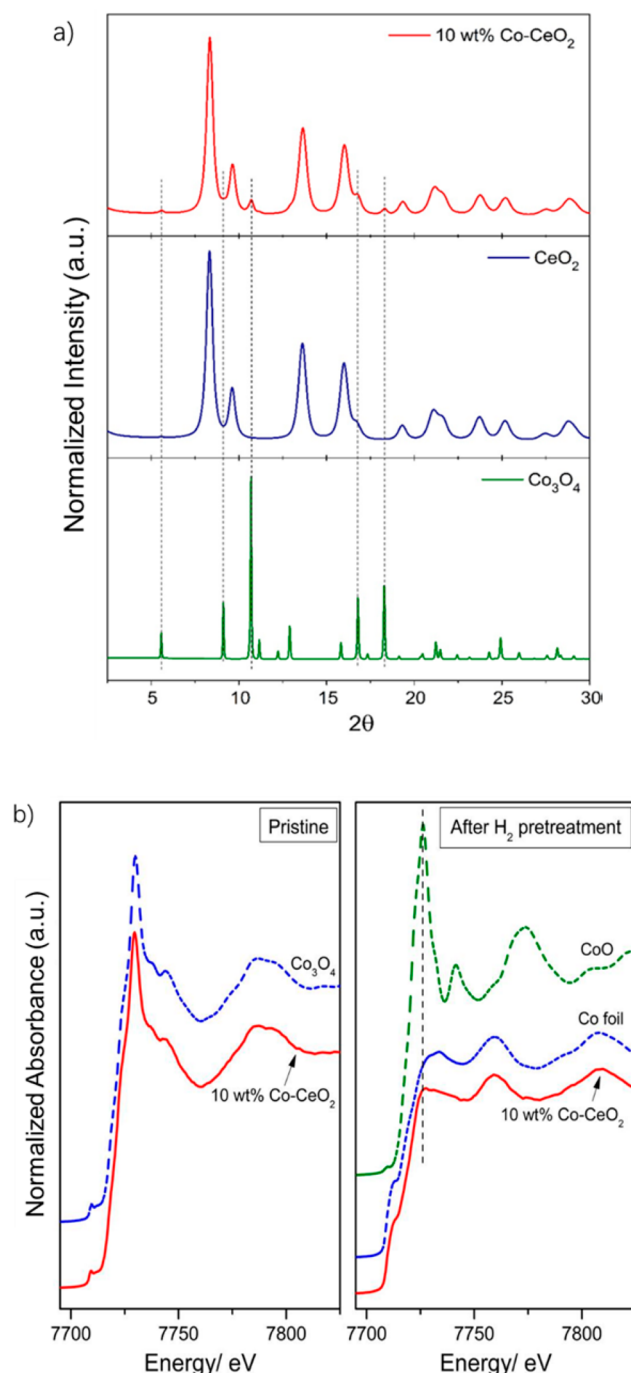
Figure 1. (a) Ex situ XRD patterns of 10 wt % Co−CeO$_2$ catalyst in comparison to bulk Co$_3$O$_4$ and CeO$_2$ standards. (b) Ex situ XANES of 10 wt % Co−CeO$_2$, as prepared and after H$_2$ pretreatment in comparison to Co metal, CoO, and Co$_3$O$_4$ standards.

decrease with the increasing metal loading, primarily due to the covering of adsorption sites of ceria by the increased amount of Co. XANES measurements for the 10 wt % catalyst were performed for the as-prepared and H$_2$ pretreated catalysts (Figure 1b). The as-prepared catalyst was identified as Co$_3$O$_4$ as evident from the similarity of its XANES spectrum with that of the Co$_3$O$_4$ reference. After H$_2$ treatment, the significant decrease of the Co$_3$O$_4$ main absorption peak accompanied by the appearance of metallic Co pre-edge feature indicates the transformation of Co$_3$O$_4$ to Co^0, while a small amount of Co^{2+}

(marked by the vertical line in Figure 1b) still remained after the pretreatment.

HRTEM and STEM images show well-distributed and homogeneous nanoparticles for the prepared $Co-CeO_2$ samples, except for the sample with an admetal loading of 30 wt %, in which Co agglomeration takes place (Figure S2, top panel). Separated particles Co_3O_4 and CeO_2 can be identified, and they are in close contact at a sharp interface, as shown in Figure 2 for the 10 wt % $Co-CeO_2$ catalyst. The morphology of the Co_3O_4 is hemispherical and appears to be anchored to CeO_2.
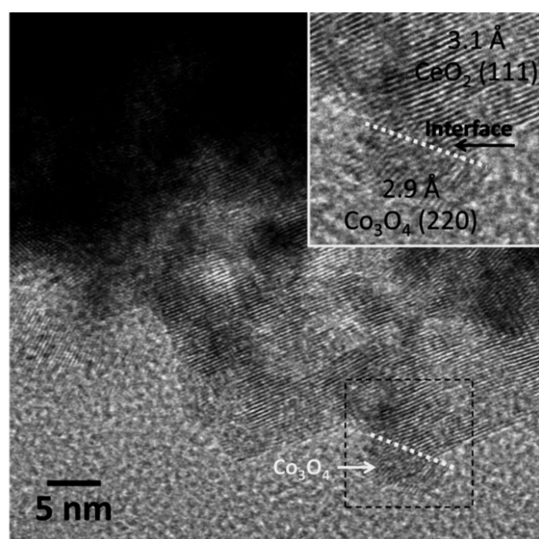

Figure 2. HRTEM images of as-prepared 10 wt % $Co-CeO_2$ sample.

Interaction of CoO_x-CeO_2 with Pure CH_4. Previous studies examining the interaction of methane with $CoO_x-CeO_2(111)$ show chemisorption of the CH_4 molecule at room temperature. However, the amount of CH_4 fully dissociated at room temperature was small, and there was no change in the oxidation state of the cobalt or cerium cations. The reduction of these cations was observed above 400 °C.[32] Using this information as a reference, we investigated the reactivity of methane with our CoO_x-CeO_2 powder samples. Figure 3a compares the methane consumption over the 10 wt % $Co-CeO_2$ catalyst, plain CeO_2, and plain Co_3O_4 samples during the CH_4-TPR, and it manifests the importance of metal−support interactions for the methane activation. At around 500 °C, it is observed in the results shown in Figure 3a that neither the plain CeO_2 sample nor the Co_3O_4 sample shows significant and continuous CH_4 consumption during the TPR reaction as compared to the 10 wt % $Co-CeO_2$ sample. Plain CeO_2 reacts with CH_4 mainly above 600 °C, which is also consistent with literature-reported results,[36−38] while the Co_3O_4 exhibits a sharp consumption peak of CH_4, but the onset temperature at ~575 °C is much higher than that seen for the 10 wt % $Co-CeO_2$ catalyst ~520 °C, and the methane level soon resumes after the initial uptake (also see Figure 3d), which is the result of a rapid deactivation of the sample from carbon deposition owing to the absence of an oxidative substrate. This result demonstrates that only cobalt in combination with ceria performs the most effective activation of methane, which highlights the critical role of metal−support interactions.

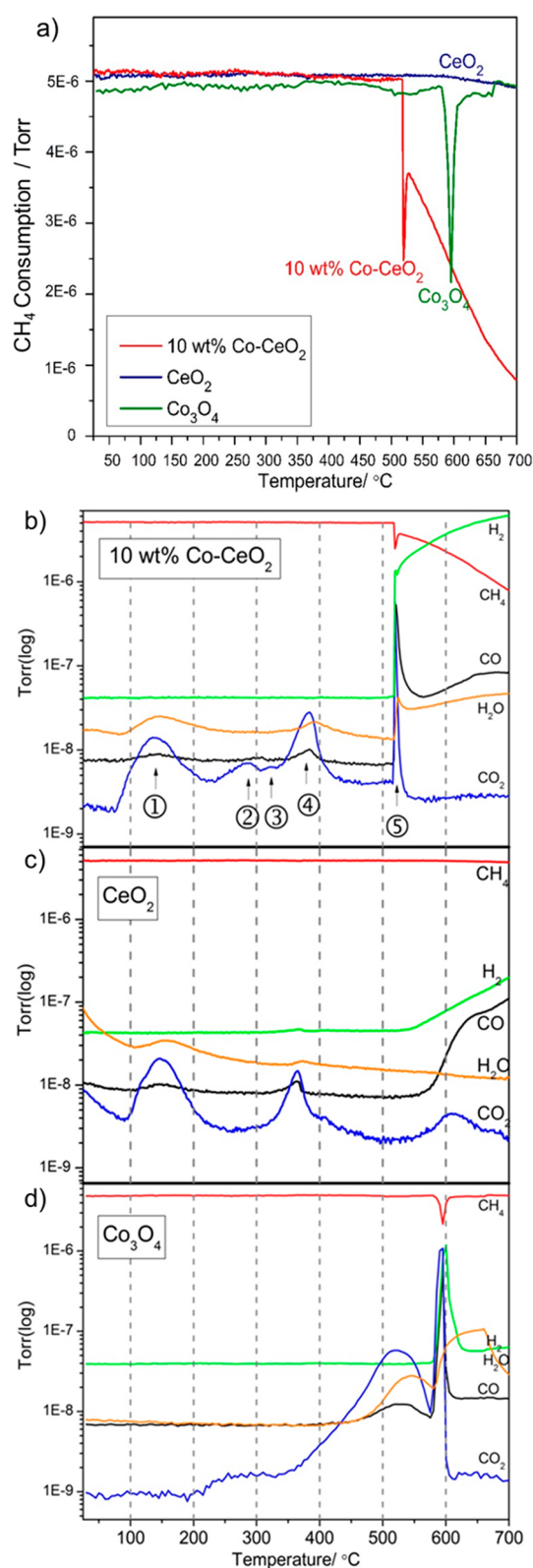Figure 3b depicts gas evolution during the CH_4-TPR over a 10 wt % $Co-CeO_2$ sample. The production of CO_2, CO, and

Figure 3. (a) CH_4 consumption on 10 wt % $Co-CeO_2$, plain CeO_2, and Co_3O_4 during CH_4-TPR and gas profiles of CH_4-TPR over (b) 10 wt % $Co-CeO_2$, (c) plain CeO_2, and (d) plain Co_3O_4.

H_2O was identified at lower temperatures, implying a reduction process of the sample by CH_4. The first release of CO_2 and H_2O at around 140 °C (peak 1) can be attributed to the desorption of surface adsorbed CO_2 and H_2O from the air on

ceria defects, which can also be observed in a plain CeO_2 CH_4-TPR experiment (Figure 3c). Then the three CO_2 peaks (2−4) overlapping with each other at a temperature range from 250 to 400 °C are due to a series of reductions occurred on the catalyst ($Co_3O_4 \rightarrow CoO \rightarrow Co$, $CeO_2 \rightarrow CeO_x$), which can be verified by the CH_4-TPR in situ XRD results (Figures 4 and 5).
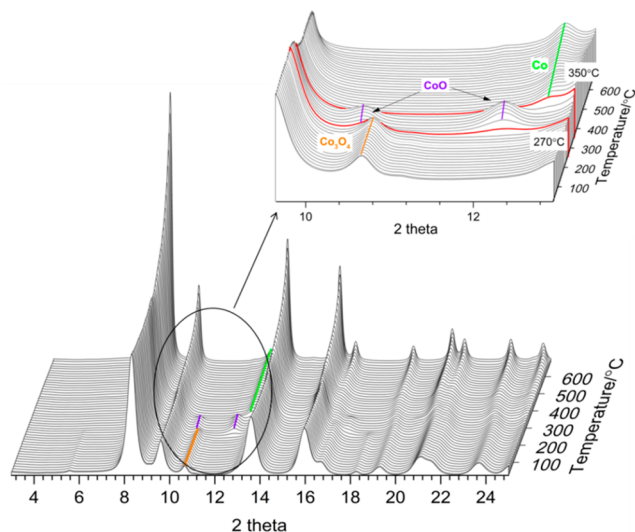
Figure 4. Sequential in situ XRD patterns collected during the CH_4-TPR on a 10 wt % Co−CeO_2 catalyst.
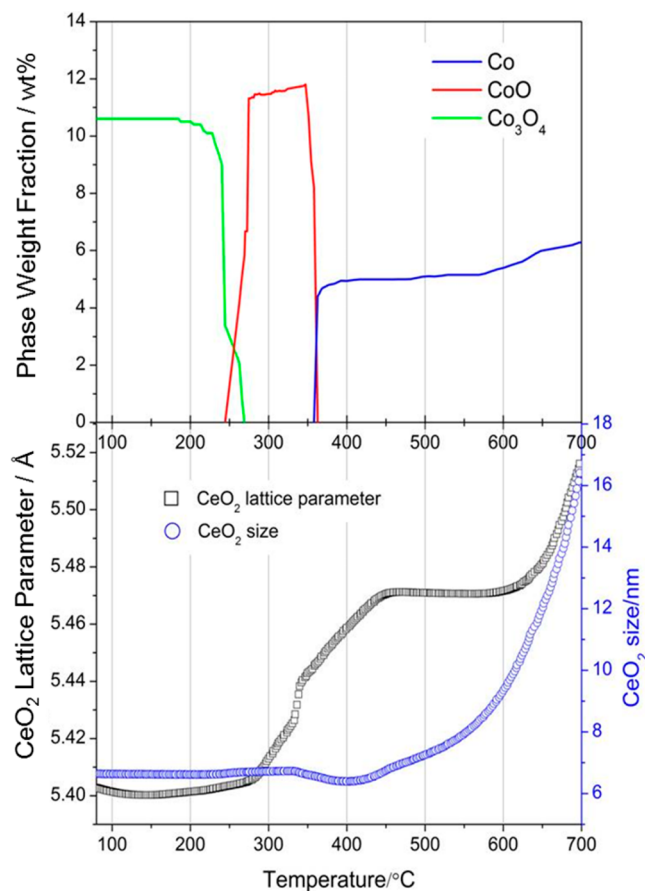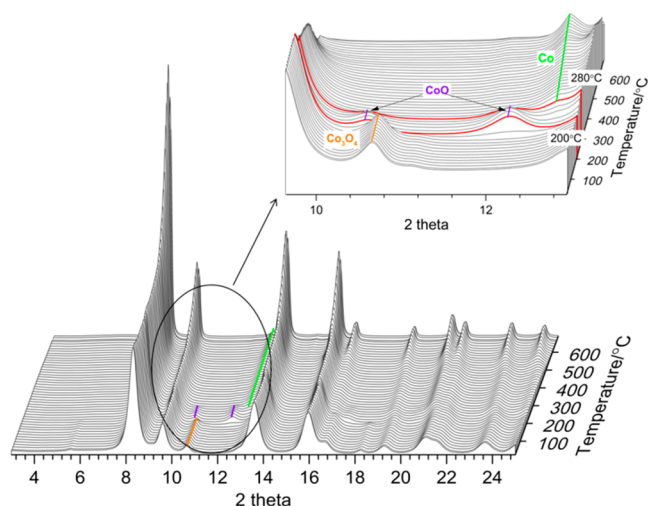

Figure 5. Co-containing phases weight fraction (top panel), CeO_2 particle size (bottom panel), and lattice parameter (bottom panel) change during the CH_4-TPR.

The decomposition of methane took place on the metallic cobalt near 520 °C (peak 5), as evidenced by the sharp methane consumption peak along with a continuous methane reaction tail and H_2 emission until 700 °C. The simultaneous production of CO and H_2O indicates the participation of O from ceria into CH_4 decomposition, which sustains the continuous reaction without significant surface deactivation by carbon deposition.[36−39] The CO_2 release at around 530 °C in Figure 3d corresponds to the reduction of Co_3O_4, which appears to be at higher temperature than that of 10 wt % Co−CeO_2 catalyst, indicating a better reducibility of cobalt phase when it is anchored onto a ceria support. Additionally, we also performed tests for a mechanical mixture of Co_3O_4 and CeO_2 and found a much lower activity than for the Co−CeO_2 catalyst, implying that indeed we have synergistic interactions in our samples.

In situ XRD patterns for the CH_4-TPR are displayed in Figure 4. These data clearly show the evolution of the cobalt oxidation state during the reduction. The diffraction pattern was quantified by Rietveld refinement as a function of temperature (Figure 5). It can be seen from Figures 4 and 5 that a first phase transition of Co_3O_4 to CoO took place around 270 °C, and CoO was further reduced to Co^0 near 350 °C, which is consistent with the CO_2 release peaks in Figure 3b. The lower panel of Figure 5 depicts the ceria lattice parameter and particle size variations during the CH_4-TPR process. In addition to the thermal expansion, when ceria is reduced, the increased ionic radius of reduced Ce^{3+}, together with the electrostatic repulsion between oxygen vacancies and the surrounding cations could expand the ceria lattice abruptly.[40] Thus, the sharp increase of CeO_2 lattice parameter between 300 and 450 °C can be regarded as the partial reduction of ceria layers near the surface, and this near surface reduction is shown to be right after the completion of Co_3O_4 reduction to CoO. The second steep increase of the CeO_2 lattice parameter starting above 600 °C can be attributed to the further bulk reduction of CeO_2 at higher temperatures.[41−43]

Interaction of CoO_x−CeO_2 with Pure H_2. To establish patterns in reactivity, it is important to compare the reducibility of the catalysts under methane and hydrogen. To investigate the reducibility of the samples under H_2 atmosphere and determine the appropriate catalyst pretreatment temperature for the DRM reaction, in situ H_2-TPR XRD measurements were also performed on the 10 wt % Co−CeO_2 catalyst. The results in Figure 6 reveal a similar Co_3O_4 reduction to metallic cobalt as that detected during the CH_4-TPR, and the temperatures for $Co_3O_4 \rightarrow CoO \rightarrow Co^0$ transitions in a H_2 atmosphere, around 200 and 280 °C, respectively, are both lower than those in a CH_4 environment (270 and 350 °C, see Figure 4). Furthermore, Rietveld refinement of the H_2-TPR diffraction peaks in Figure 7 points to a two-stage reduction of CeO_2. The first one starting around 200 °C, right after the CoO formation, corresponds to the partial reduction of Ce^{4+} near the surface, and the second one around 450 °C could be attributed to a further bulk reduction of the CeO_2. The Rietveld refinement results suggest the appropriate H_2 pretreatment temperature to be 550 °C. From Figure 7, one sees that at around 450 °C, a metallic Co phase starts to develop significantly, but when the temperature reached up to 550 °C, CeO_2 particle size also increases rapidly to 40 nm until 700 °C. This substantial increase of the ceria particle size would significantly lower the metal dispersion and decrease the amount of cobalt and ceria interface, which results in the poor

Figure 6. Sequential in situ XRD patterns acquired while performing the H_2-TPR on a 10 wt % Co–CeO$_2$ catalyst.
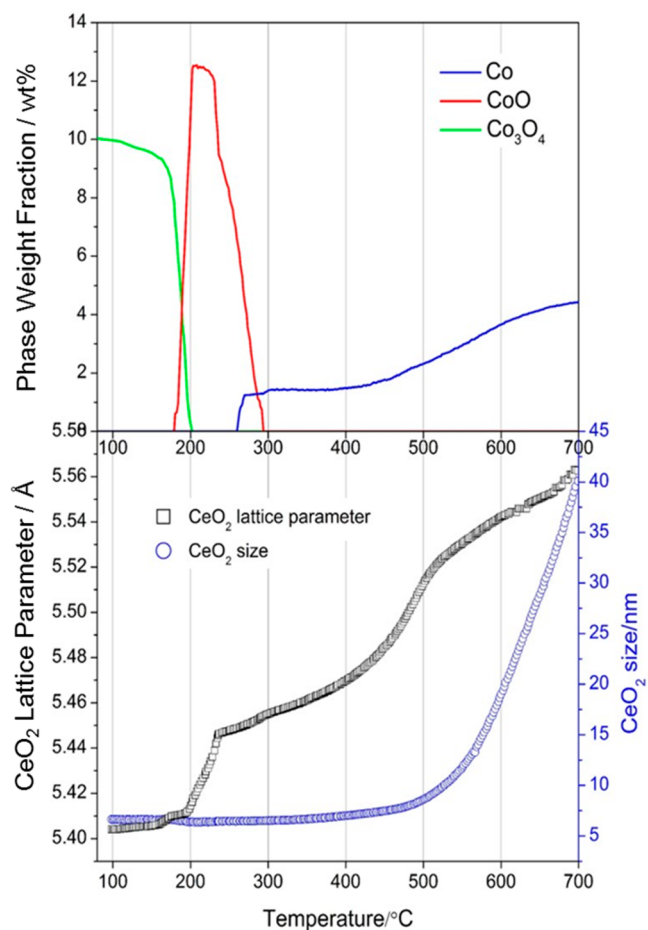

Figure 7. Cobalt-containing phases as weight fractions (top panel), CeO_2 particle size (bottom panel), and ceria lattice parameter (bottom panel) as a function of temperature during the H_2-TPR on a 10 wt % Co–CeO$_2$ catalyst.

catalytic activity of the sample pretreated at 600 and 700 °C (Figure S3) for the DRM reaction.[44]

Catalytic Performance and In Situ Structural Change of Co–CeO$_{2-x}$ under the DRM Reaction Conditions. The catalytic activities for different Co loadings (2, 4, 6, 8, 10, 20, 30

wt %)were compared through normalized H_2 and CO production at 500 °C (normalized by weight of the catalyst and cobalt loadings), and the results are shown in Figure S4. A catalyst with a 10 wt % Co–CeO$_2$ composition has the highest activity among these samples. For the 10 wt % Co–CeO$_2$ sample at 500 °C, the conversion of CH_4 is around 8% and CO_2 is around 11%; the reaction rate is 1.51×10^{-4} mol/s for CH_4 and 2.07×10^{-4} mol/s for CO_2; the turnover frequency (TOF) is approximately131 s^{-1} for CH_4 and 180 s^{-1} for CO_2, and the H_2 selectivity is 25%, with carbon ratio at around 96% (see the Supporting Information for corresponding calculations). The conversion measured for our best 10 wt % Co–CeO$_2$ catalyst was close to the thermodynamic limit expected at 500 °C.[20,22]

The in situ XRD measurement for the DRM reaction was then performed on the 10 wt % Co–CeO$_2$ catalyst. The sample was first prereduced in H_2 at 550 °C, and the DRM reaction was carried out after the gas was switched to a CO_2, CH_4, and He mixture at room temperature. The in situ XRD profile recorded in Figure 8 reveals that Co_3O_4 was reduced to metallic
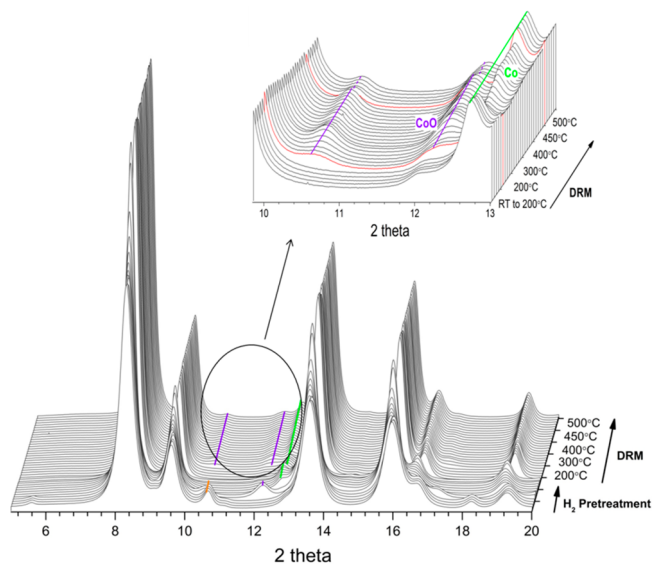
Figure 8. Sequential in situ XRD patterns collected during the DRM reaction on a 10 wt % Co–CeO$_2$ catalyst.
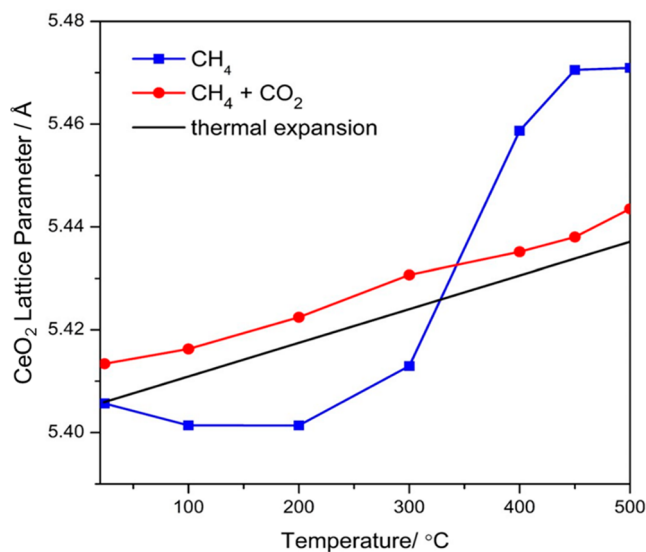
Co through a CoO transition phase during the H_2 pretreatment, which is consistent with the H_2-TPR experiment. After a switch to DRM reactant gases, the CoO reemerged at 200 °C and remained intact until the temperature warmed to 500 °C, as evident in the middle panel of Figure 9. Starting from 500 °C, a significant amount of CoO was gradually reduced to metallic Co. One can correlate this phase development to the gas evolution monitored by the mass spectrometer shown in Figure 9 (top panel), where apparent consumption of CO_2 and CH_4 as well as the production of CO and H_2 were observed when the temperature reached 500 °C, and this clearly demonstrates the importance of metallic Co for the production of syngas. Moreover, the larger expansion of the CeO_2 lattice in the temperature range from 200 to 300 °C and from 450 to 500 °C than that in temperature range from 300 to 450 °C in Figure 9 (bottom panel), suggests a partial reduction of Ce^{4+} into Ce^{3+}. However, when the CeO_2 lattice parameter of the 10 wt % Co–CeO$_2$ sample under the DRM reaction is compared with the thermal expansion of bulk CeO_2 (linear thermal
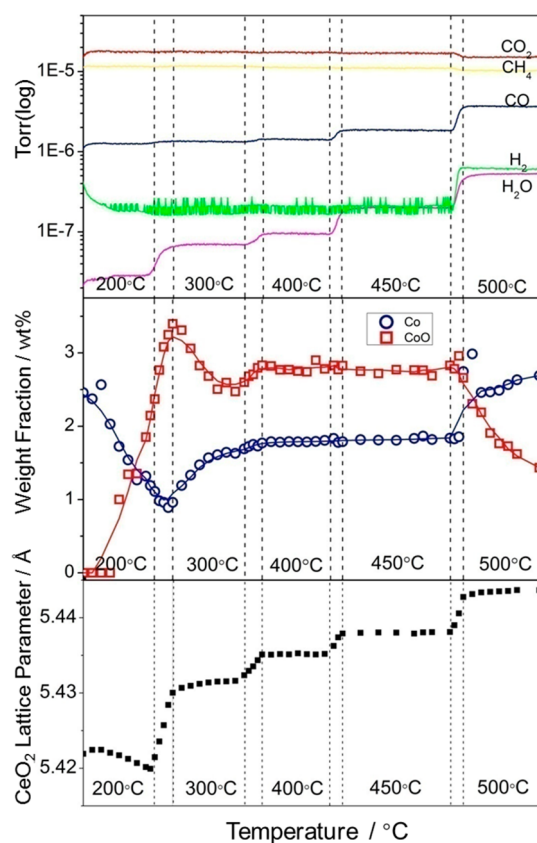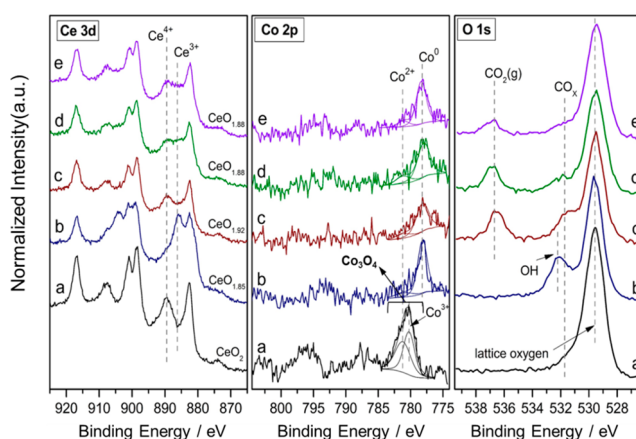
Figure 9. Top panel: Gas composition measured with a mass spectrometer at the outlet of the reactor during the DRM reaction at different temperatures. In the reactor, 4 mg of the 10 wt % Co–CeO$_2$ catalyst was exposed to a reaction mixture of 2 mL/min CH$_4$, 2 mL/min CO$_2$, and 6 mL/min He. Middle and bottom: Results from in situ XRD after the H$_2$ pretreatment for the corresponding phase evolution of CoO and Co and the CeO$_2$ lattice parameter at different temperatures under the DRM reaction.

Figure 10. Comparison of CeO$_2$ lattice parameter changes of the 10 wt % Co–CeO$_2$ catalyst under CH$_4$ atmosphere and during the DRM reaction as a function of temperature; a bulk CeO$_2$ lattice thermal expansion line is also provided for reference.

Figure 11. AP-XPS profiles in the Ce 3d, Co 2p, and O 1s regions of 10 wt % Co–CeO$_2$ catalyst (a) as prepared at 25 °C, (b) cooled to 25 °C after 1 h of H$_2$ pretreatment at 550 °C, and during the DRM reaction (75 mTorr of CO$_2$ + 75 mTorr of CH$_4$): (c) at 25 °C, (d) 400 °C, and (e) 500 °C.

expansion coefficient ~1.21 × 10^{-5}), as shown in Figure 10, a nearly thermal expansion rate of CeO$_2$ lattice can be observed during the DRM reaction, and the lattice parameter under reaction condition is larger than that of bulk CeO$_2$.[45] This indicates the formation of a partially reduced CeO$_{2-x}$ phase under a redox equilibrium during the DRM reaction. Additionally, when the CeO$_2$ lattice parameter was compared in CH$_4$ and CO$_2$ atmosphere with that in CH$_4$ atmosphere, a decreased CeO$_2$ lattice parameter was observed between 300 and 500 °C under the DRM conditions, and this can be explained by the presence of CO$_2$ which, when activated, heals a fraction of oxygen vacancies in the prereduced CeO$_{2-x}$, implying the partial reoxidation of Ce^{3+} to Ce^{4+} during the DRM reaction.

Methane Dry Reforming Reaction Characterized by AP-XPS. As the information retrieved from the in situ XRD is primarily bulk-sensitive and identifies the crystalline phase of the catalysts, an AP-XPS experiment was conducted for the 10 wt % Co–CeO$_2$ sample to provide further information regarding the surface oxidation state of the catalysts under reaction conditions but at moderate pressures. Results in Figure 11 confirm the partial reduction of Ce^{4+} to a mixture of Ce^{3+} and Ce^{4+}. After the gas was switched to CH$_4$ and CO$_2$, partial reoxidation of prereduced Ce^{3+} to Ce^{4+} is evident even at room temperature, as seen from the attenuated intensity of Ce^{3+} peak

as well as the growing intensity of characteristic Ce^{4+} feature at 25 °C under the DRM conditions. However, as the sample was heated to 400 °C, Ce^{4+} was slightly reduced and remained stable when the temperature increased to 500 °C. In the Co 2p region, Co$_3$O$_4$ was reduced to metallic Co after H$_2$ pretreatment (Co 2p: a → b). Changing the gas atmosphere to DRM conditions (CO$_2$ + CH$_4$) caused the slight reoxidation of metallic Co (Co 2p: b → d), but it returned predominantly to Co^0 as the reaction proceeded to 500 °C (Co 2p: d → e). The relative percentages for Co species are listed in Table 1, and

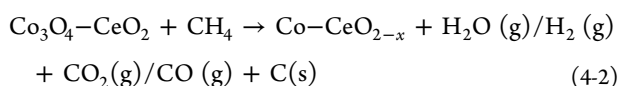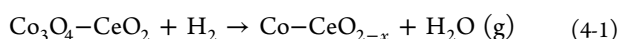**Table 1. Relative Percentages of Metallic Co Derived from Co 2p AP-XPS Data**

| condition	25 °C (after H$_2$ pretreatment)	25 °C (DRM)	400 °C (DRM)	500 °C (DRM)
Co^0 (% area)	87.34	84.57	80.67	86.32

this trend for the variation of the Co oxidation state is in agreement with our in situ XRD studies. The O 1s data also shows small amount of CO_x species that present on the catalyst surface, implying CO_x (e.g., carbonate, carboxyl, bicarbonate) as a possible reaction intermediate.

■ DISCUSSION

The Structural and Chemical State of Co and Ceria under Reaction Conditions. As mentioned in the Introduction, several models or hypothesis have been proposed to explain the performance of Co-ceria catalysts during the DRM reaction.[24,31] Our in situ studies with XRD and XPS point to dynamic changes of catalysts that undergo structural and chemical transformations upon reaction with CH_4 and CO_2 at elevated temperatures. From the results of both H_2 and CH_4-TPR, the Co_3O_4 in the as-prepared Co-ceria sample experienced two-step phase transformations from Co_3O_4 to CoO and then to metallic Co, whereas CeO_2 was partially reduced to CeO_{2-x} (Figures 5 and 7). These chemical changes can be expressed as

$$Co_3O_4-CeO_2 + H_2 \rightarrow Co-CeO_{2-x} + H_2O \text{ (g)} \quad (4\text{-}1)$$

$$Co_3O_4-CeO_2 + CH_4 \rightarrow Co-CeO_{2-x} + H_2O \text{ (g)}/H_2 \text{ (g)}$$
$$+ CO_2(g)/CO \text{ (g)} + C(s) \quad (4\text{-}2)$$

After the gas was switched to a mixture of CO_2 and CH_4, CeO_{2-x} was first reoxidized via the activation of CO_2 even at room temperature, as evidenced in Figure 11c, and significant fraction of oxygen vacancies in CeO_{2-x} were healed by CO_2 as described below:

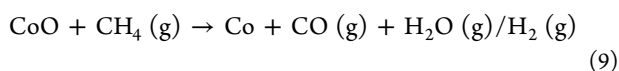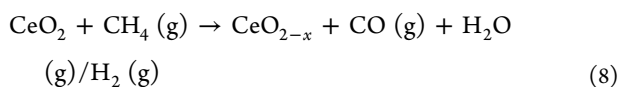$$Vac + CO_2 \text{ (g)} \rightarrow O-Vac + CO \text{ (g)} \quad (5)$$
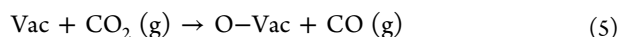
On the other hand, the reemergence of CoO at 200 °C (Figures 8 and 9), implies the strong oxophilic nature of cobalt leads to the formation of CoO through an oxygen transfer from either CO_2 or the lattice O of ceria, which can be interpreted by the following possible reactions:

$$Co + CO_2 \text{ (g)} \rightarrow CoO + CO \text{ (g)} \quad (6)$$

and/or

$$Co + O-Vac \rightarrow CoO + Vac \quad (7)$$
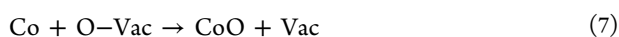
At temperatures above 200 °C, the reduction of the catalyst evolves as a result of the CH_4 activation:

$$CeO_2 + CH_4 \text{ (g)} \rightarrow CeO_{2-x} + CO \text{ (g)} + H_2O$$
$$\text{(g)}/H_2 \text{ (g)} \quad (8)$$

$$CoO + CH_4 \text{ (g)} \rightarrow Co + CO \text{ (g)} + H_2O \text{ (g)}/H_2 \text{ (g)} \quad (9)$$

In general, the catalytic oxidation cycle led by the activation of CO_2, reactions 5 and (6), and the reduction cycle led by the activation of CH_4, reactions 8 and 9, compete with each other during the DRM process, with the catalyst's oxidation state evolving between 300 and 500 °C depending on the reaction conditions(Figure 9). At temperatures below 500 °C, the oxidative effect by CO_2 activation dominates and most of the cobalt phase remains as Co^{2+}. At 500 °C, the reduction cycle imposed by methane conversion becomes significant, and metallic Co starts to exceed Co^{2+}. The formation of a substantial amount of metallic Co simultaneously leads to the

largely increased catalytic activity (Figure 9 top panel) through the reactions:

$$Co-CH_4 \rightarrow Co-C(a) + 2H_2 \text{ (g)} \quad (10)$$

$$C(a) + O-Vac \rightarrow CO \text{ (g)} + Vac \quad (11)$$
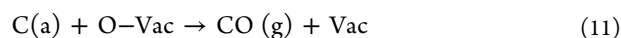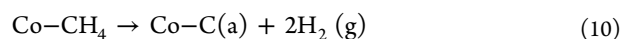
Our in situ studies indicate that a balance between reduction by CH_4 and oxidation by CO_2 must be taken into consideration when optimizing or designing new metal/oxide catalysts for the DRM process. In general, terms the low temperature activation of CH_4 on the powders of $Co-CeO_2$ is comparable to the results found in our previous studies for the model $Co-CeO_2(111)$ system. Under reaction conditions the nature of the active state of Co and the extent of the reduction in ceria are similar in both cases. Thus, similar chemical pathways that convert $CH_4 + CO_2$ probably occur on the model and powder systems. This is probably a consequence of the fact that CeO_2 (111) is the most common surface exposed in the powder catalysts.

Coke Tolerance and Comparison with Ni-Based Catalyst. Owing to the existence of Co^{2+} until the end of the experiment at 500 °C, neither deposited coke (see Figure S2, bottom panel, HRTEM image of the postrun sample) nor crystallized cobalt carbide (absence of cobalt carbide peaks in Figure 8) is found during the DRM reaction, which is different from the behavior of Ni observed in $Ni-CeO_2$ catalyst.[46−48] Metastable cobalt carbides (Co_2C and Co_3C) form and maintain at relatively low temperature, both between 450 and 500 °C.[49−51] However, a small amount of cobalt still remains as Co^{2+} in our reaction, even at 500 °C. These oxygen atoms in the metal phase could combine with the surface carbon resulting from CH_4 dissociation or CO disproportionation and suppress the formation of cobalt carbides and coke.

$$Co-O + C(a) \rightarrow Co + CO \text{ (g)} \quad (12)$$
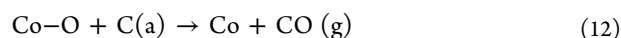
Additionally, it has been reported that Ni-based catalysts show a higher C−H bond activation rate than that of Co catalysts at a lower temperature range, while Co exhibits better performance at higher temperatures.[26] Our previous results on a model catalytic system also show that metallic Co in close contact with ceria has lower methane activation barrier than the case of Ni.[32] In this study, we also compared the activity of 10 wt % $Co-CeO_2$ and 10 wt % $Ni-CeO_2$ prepared by the same wetness impregnation method and found that Ni exhibited better activity than Co below 500 °C (Figure S5) but deactivated rapidly as temperature went high. However, the activity and stability of $Co-CeO_2$ catalysts at 500 °C is much better than that of Ni catalyst and maintains active up to 700 °C (Figures S5 and S6). At lower temperature range, part of the cobalt exists as cobalt(II) oxide and the amount of the metallic active phase decreases, which accounts for the lower C−H bond activation rate of Co catalysts than that of Ni catalysts, but as temperature increases to 500 °C, more metallic Co is produced and readily participates into the direct dissociation of CH_4 (see eq 10). The interaction between ceria and Co as well as the better oxophilicity of Co play the essential roles here to achieve the better activity and stability of the $Co-CeO_2$ sample.

In several of the catalytic measurements the appearance of H_2O as a byproduct of the RWGS is prevalent for this process, hindering the ability to produce H_2 selectively. In addition to the presence of H_2O, its dissociated −OH form may be a critical component on the surface. It is very likely that both Co metal and Ce^{3+} are very efficient at dissociation of H_2O and the

resulting hydroxylation of surface sites may occur. This aspect though not studied systematically here may influence possible pathways to produce CO and H_2 through steam reforming like processes.

Metal−support Interactions and the Important Role of Ceria. The H_2-TPR study of plain CeO_2 revealed that the reduction of surface ceria (calcined at 400 °C) began at 200 °C and stabilized after 400 °C; further bulk reduction of ceria requires the temperature above 650 °C.[41−43] In contrast, the in situ H_2-TPR experiment of our 10 wt % Co−CeO_2 sample shows that the surface reduction of ceria takes place between 200 and 230 °C, and the bulk reduction occurs around 450 °C (Figure 7). At the same time, the reduction of Co_3O_4 in our sample experiences two steps, from Co_3O_4 to CoO at 200 °C and from CoO to metallic Co at 280 °C (Figure 7) in H_2 atmosphere, whereas in the literature, it has been reported that the reduction of bulk Co_3O_4 initiated at around 200 °C, with the majority of the metallic Co phase stabilized above 330 °C.[52−55] The high activity of the reducible ceria support to dissociate H_2 with subsequent transfer of the H atoms to cobalt oxide, could facilitate a reduction of $Co^{2+,3+}$ into Co^0.[56,57] Compared with other supports like alumina, which forms a weakly reducible $CoAl_2O_4$ phase and hinders the reduction process, or titania, which requires high reduction temperature to obtain an active phase, the ceria support interacts with cobalt phases and promotes the reduction process of both ceria and cobalt.[56−60] Additionally, the oxygen vacancies created in the ceria lattice will stabilize the supported metals, herein making ceria an advantageous support for the catalyst.[61,62]

CONCLUSION

We have carefully examined the reaction of methane with Co−CeO_x catalysts and the dry reforming using several in situ experimental methods. We have extended and validated our previous studies on well-defined planar Co−CeO_2(111) model surfaces to power catalysts in more realistic reaction conditions. The role of each component under reaction conditions is complex and dynamic. Clear transitions of $Co_3O_4 \rightarrow CoO \rightarrow Co$ and $Ce^{4+} \rightarrow Ce^{3+}$ occur upon exposure to pure methane at temperatures in the range between 200 and 350 °C. CO_2 dissociates on the reduced surfaces and acts as an oxidant agent, converting part of the Co to CoO and Ce^{3+} to Ce^{4+}. The interaction between the Co and ceria and the role of the reducible oxide are essential for a complex series of pathways that lead to the production of CO and H_2. Our in situ results indicate that under the DRM reaction conditions, when product formation is optimum, the active state of the catalyst is predominantly metallic Co, with a small presence of CoO, supported on a partially reduced ceria (Ce^{3+}/Ce^{4+}). The Co component is responsible for the activation of CH_4, mediated through CO_2 donating O through the ceria support.

ASSOCIATED CONTENT

Ⓢ Supporting Information

The Supporting Information is available free of charge on the ACS Publications website at DOI: 10.1021/acscatal.7b03640.

> Ex situ XRD patterns of fresh catalysts, including 2, 4, 6, 8, 10, and 30 wt % Co on CeO_2; XRD refinement result and BET surface area of the prepared catalysts; STEM image of 30 wt % Co−CeO_2 catalyst and HRTEM image of 8 wt % postexperiment catalyst; CO production of 10

wt % Co−CeO_2 after pretreatment at different temperatures; normalized CO and H_2 production over various cobalt loading catalysts at 500 °C during the DRM reaction (taking into the account of the weight of the catalyst and the cobalt loading); comparison of catalytic activities of the 10 wt % Ni−CeO_2 and 10 wt % Co−CeO_2 during the DRM reaction; 10 wt % Co−CeO_2 stability test; equations used for the calculations of the TOF and conversions (PDF)

■ AUTHOR INFORMATION

Corresponding Authors
*E-mail: ssenanay@bnl.gov.
*E-mail: taejin.kim@stonybrook.edu.

ORCID ⊙
Zongyuan Liu: 0000-0001-8526-5590
Dimitriy Vovchok: 0000-0001-6423-7566
José A. Rodriguez: 0000-0002-5680-4214
Jordi Llorca: 0000-0002-7447-9582
DoHeui Kim: 0000-0003-3870-1606
Anatoly I. Frenkel: 0000-0002-5451-1207
Taejin Kim: 0000-0002-0096-303X
Sanjaya D. Senanayake: 0000-0003-3991-4232

Notes
The authors declare no competing financial interest.

■ REFERENCES

(1) Babarao, R.; Jiang, J. Upgrade of natural gas in rhozeolite-like metal-organic framework and effect of water: a computational study. *Energy Environ. Sci.* **2009**, *2*, 1088−1093.

(2) Tippayawong, N.; Thanompongchart, P. Biogas quality upgrade by simultaneous removal of CO_2 and H_2S in a packed column reactor. *Energy* **2010**, *35*, 4531−4535.

(3) Kismurtono, M. Upgrade biogas purification in packed column with chemical absorption of CO_2 for energy alternative of small industry (UKM-Tahu). *Int. J. Eng. Technol.* **2011**, *11*, 83−86.

(4) Ghorbanzadeh, A.; Norouzi, S.; Mohammadi, T. High energy efficiency in syngas and hydrocarbon production from dissociation of CH_4−CO_2 mixture in a non-equilibrium pulsed plasma. *J. Phys. D: Appl. Phys.* **2005**, *38*, 3804.

(5) Dry, M.; Steynberg, A. Commercial FT process applications. *Stud. Surf. Sci. Catal.* **2004**, *152*, 406−481.

(6) Budiman, A. W.; Song, S.-H.; Chang, T.-S.; Shin, C.-H.; Choi, M.-J. Dry reforming of methane over cobalt catalysts: a literature review of catalyst development. *Catal. Surv. Asia* **2012**, *16*, 183−197.

(7) Wang, S.; Lu, G.; Millar, G. J. Carbon dioxide reforming of methane to produce synthesis gas over metal-supported catalysts: state of the art. *Energy Fuels* **1996**, *10*, 896−904.

(8) Bradford, M.; Vannice, M. CO_2 reforming of CH_4. *Catal. Rev.: Sci. Eng.* **1999**, *41*, 1−42.

(9) Bradford, M. C.; Vannice, M. A. Catalytic reforming of methane with carbon dioxide over nickel catalysts I. Catalyst characterization and activity. *Appl. Catal., A* **1996**, *142*, 73−96.

(10) Cavenati, S.; Grande, C. A.; Rodrigues, A. E. Separation of CH_4/CO_2/N_2 mixtures by layered pressure swing adsorption for upgrade of natural gas. *Chem. Eng. Sci.* **2006**, *61*, 3893−3906.

(11) Belmabkhout, Y.; De Weireld, G.; Sayari, A. Amine-bearing mesoporous silica for CO_2 and H2S removal from natural gas and biogas. *Langmuir* **2009**, *25*, 13275−13278.

(12) Fan, M. S.; Abdullah, A. Z.; Bhatia, S. Catalytic technology for carbon dioxide reforming of methane to synthesis gas. *ChemCatChem* **2009**, *1*, 192−208.

(13) Peters, R. L. The greenhouse effect and nature reserves. *BioScience* **1985**, *35*, 707−717.

(14) Rodhe, H. A comparison of the contribution of various gases to the greenhouse effect. *Science* **1990**, *248*, 1217−1219.

(15) Huang, A.; Xia, G.; Wang, J.; Suib, S. L.; Hayashi, Y.; Matsumoto, H. CO_2 reforming of CH_4 by atmospheric pressure ac discharge plasmas. *J. Catal.* **2000**, *189*, 349−359.

(16) Cavenati, S.; Grande, C. A.; Rodrigues, A. E. Upgrade of methane from landfill gas by pressure swing adsorption. *Energy Fuels* **2005**, *19*, 2545−2555.

(17) Lavoie, J.-M. Review on dry reforming of methane, a potentially more environmentally-friendly approach to the increasing natural gas exploitation. *Front. Chem.* **2014**, *2*, 81.

(18) Hou, Z.; Chen, P.; Fang, H.; Zheng, X.; Yashima, T. Production of synthesis gas via methane reforming with CO_2 on noble metals and small amount of noble-(Rh-) promoted Ni catalysts. *Int. J. Hydrogen Energy* **2006**, *31*, 555−561.

(19) Nematollahi, B.; Rezaei, M.; Khajenoori, M. Combined dry reforming and partial oxidation of methane to synthesis gas on noble metal catalysts. *Int. J. Hydrogen Energy* **2011**, *36*, 2969−2978.

(20) Liu, Z.; Grinter, D. C.; Lustemberg, P. G.; Nguyen-Phan, T.-D.; Zhou, Y.; Luo, S.; Waluyo, I.; Crumlin, E. J.; Stacchiola, D. J.; Zhou, J.; Carrasco, J.; Busnengo, H. F.; Ganduglia-Pirovano, M. V.; Senanayake, S. D.; Rodriguez, J. A. Dry Reforming of Methane on a Highly-Active Ni-CeO$_2$ Catalyst: Effects of Metal-Support Interactions on C−H Bond Breaking. *Angew. Chem.* **2016**, *128*, 7581−7585.

(21) Rostrupnielsen, J.; Hansen, J. B. CO_2-reforming of methane over transition metals. *J. Catal.* **1993**, *144*, 38−49.

(22) Pakhare, D.; Spivey, J. A review of dry (CO_2) reforming of methane over noble metal catalysts. *Chem. Soc. Rev.* **2014**, *43*, 7813−7837.

(23) Ayodele, B. V.; Khan, M. R.; Lam, S. S.; Cheng, C. K. Production of CO-rich hydrogen from methane dry reforming over lanthania-supported cobalt catalyst: kinetic and mechanistic studies. *Int. J. Hydrogen Energy* **2016**, *41*, 4603−4615.

(24) Ayodele, B. V.; Khan, M. R.; Cheng, C. K. Catalytic performance of ceria-supported cobalt catalyst for CO-rich hydrogen production from dry reforming of methane. *Int. J. Hydrogen Energy* **2016**, *41*, 198−207.

(25) AlSabban, B.; Falivene, L.; Kozlov, S. M.; Aguilar-Tapia, A.; Ould-Chikh, S.; Hazemann, J.-L.; Cavallo, L.; Basset, J.-M.; Takanabe, K. In-operando elucidation of bimetallic CoNi nanoparticles during high-temperature CH_4/CO_2 reaction. *Appl. Catal., B* **2017**, *213*, 177−189.

(26) Tu, W.; Ghoussoub, M.; Singh, C. V.; Chin, Y.-H. C. Consequences of Surface Oxophilicity of Ni, Ni-Co, and Co Clusters on Methane Activation. *J. Am. Chem. Soc.* **2017**, *139*, 6928−6945.

(27) San-José-Alonso, D.; Juan-Juan, J.; Illán-Gómez, M.; Román-Martínez, M. Ni, Co and bimetallic Ni−Co catalysts for the dry reforming of methane. *Appl. Catal., A* **2009**, *371*, 54−59.

(28) Ay, H.; Üner, D. Dry reforming of methane over CeO$_2$ supported Ni, Co and Ni−Co catalysts. *Appl. Catal., B* **2015**, *179*, 128−138.

(29) Zhang, J.; Wang, H.; Dalai, A. K. Development of stable bimetallic catalysts for carbon dioxide reforming of methane. *J. Catal.* **2007**, *249*, 300−310.

(30) Takanabe, K.; Nagaoka, K.; Nariai, K.; Aika, K. -i. Titania-supported cobalt and nickel bimetallic catalysts for carbon dioxide reforming of methane. *J. Catal.* **2005**, *232*, 268−275.

(31) Djinović, P.; Osojnik Črnivec, I. G.; Erjavec, B.; Pintar, A. Influence of active metal loading and oxygen mobility on coke-free dry reforming of Ni−Co bimetallic catalysts. *Appl. Catal., B* **2012**, *125*, 259−270.

(32) Liu, Z.; Lustemberg, P.; Gutiérrez, R. A.; Carey, J. J.; Palomino, R. M.; Vorokhta, M.; Grinter, D. C.; Ramírez, P. J.; Matolín, V.; Nolan, M.; Ganduglia-Pirovano, M. V.; Senanayake, S. D.; Rodriguez, J. A. In Situ Investigation of Methane Dry Reforming on Metal/Ceria(111) Surfaces: Metal−Support Interactions and C−H Bond Activation at Low Temperature. *Angew. Chem., Int. Ed.* **2017**, *56*, 13041−13046.

(33) Chupas, P. J.; Chapman, K. W.; Kurtz, C.; Hanson, J. C.; Lee, P. L.; Grey, C. P. A versatile sample-environment cell for non-ambient X-ray scattering experiments. *J. Appl. Crystallogr.* **2008**, *41*, 822−824.

(34) Toby, B. H.; Von Dreele, R. B. GSAS-II: the genesis of a modern open-source all purpose crystallography software package. *J. Appl. Crystallogr.* **2013**, *46*, 544−549.

(35) Edla, R.; Gupta, S.; Patel, N.; Bazzanella, N.; Fernandes, R.; Kothari, D.; Miotello, A. Enhanced H 2 production from hydrolysis of sodium borohydride using Co$_3$O$_4$ nanoparticles assembled coatings prepared by pulsed laser deposition. *Appl. Catal., A* **2016**, *515*, 1−9.

(36) Otsuka, K.; Ushiyama, T.; Yamanaka, I. Partial Oxidation of Methane Using the Redox of Cerium Oxide. *Chem. Lett.* **1993**, *22*, 1517−1520.

(37) Otsuka, K.; Wang, Y.; Sunada, E.; Yamanaka, I. Direct Partial Oxidation of Methane to Synthesis Gas by Cerium Oxide. *J. Catal.* **1998**, *175*, 152−160.

(38) Otsuka, K.; Sunada, E.; Ushiyama, T.; Yamanaka, I. The production of synthesis gas by the redox of cerium oxide. *Stud. Surf. Sci. Catal.* **1997**, *107*, 531−536.

(39) Zhu, T.; Flytzani-Stephanopoulos, M. Catalytic partial oxidation of methane to synthesis gas over Ni−CeO$_2$. *Appl. Catal., A* **2001**, *208*, 403−417.

(40) Marrocchelli, D.; Bishop, S. R.; Tuller, H. L.; Yildiz, B. Understanding Chemical Expansion in Non-Stoichiometric Oxides: Ceria and Zirconia Case Studies. *Adv. Funct. Mater.* **2012**, *22*, 1958−1965.

(41) López, J. M.; Gilbank, A. L.; García, T.; Solsona, B.; Agouram, S.; Torrente-Murciano, L. The prevalence of surface oxygen vacancies over the mobility of bulk oxygen in nanostructured ceria for the total toluene oxidation. *Appl. Catal., B* **2015**, *174*, 403−412.

(42) Laachir, A.; Perrichon, V.; Badri, A.; Lamotte, J.; Catherine, E.; Lavalley, J. C.; El Fallah, J.; Hilaire, L.; Le Normand, F.; Quemere, E.; Sauvion, G. N.; Touret, O. Reduction of CeO$_2$ by hydrogen. Magnetic susceptibility and Fourier-transform infrared, ultraviolet and X-ray photoelectron spectroscopy measurements. *J. Chem. Soc., Faraday Trans.* **1991**, *87*, 1601−1609.

(43) Giordano, F.; Trovarelli, A.; de Leitenburg, C.; Giona, M. A Model for the Temperature-Programmed Reduction of Low and High Surface Area Ceria. *J. Catal.* **2000**, *193*, 273−282.

(44) Soykal, I. I.; Sohn, H.; Ozkan, U. S. Effect of Support Particle Size in Steam Reforming of Ethanol over Co/CeO$_2$ Catalysts. *ACS Catal.* **2012**, *2*, 2335−2348.

(45) Mogensen, M.; Sammes, N. M.; Tompsett, G. A. Physical, chemical and electrochemical properties of pure and doped ceria. *Solid State Ionics* **2000**, *129*, 63−94.

(46) Xu, W.; Liu, Z.; Johnston-Peck, A. C.; Senanayake, S. D.; Zhou, G.; Stacchiola, D.; Stach, E. A.; Rodriguez, J. A. Steam reforming of

ethanol on Ni/CeO$_2$: reaction pathway and interaction between Ni and the CeO$_2$ support. *ACS Catal.* **2013**, *3*, 975−984.

(47) Djaidja, A.; Libs, S.; Kiennemann, A.; Barama, A. Characterization and activity in dry reforming of methane on NiMg/Al and Ni/MgO catalysts. *Catal. Today* **2006**, *113*, 194−200.

(48) Guczi, L.; Stefler, G.; Geszti, O.; Sajó, I.; Pászti, Z.; Tompos, A.; Schay, Z. Methane dry reforming with CO$_2$: A study on surface carbon species. *Appl. Catal., A* **2010**, *375*, 236−246.

(49) Nagakura, S. Study of Metallic Carbides by Electron Diffraction Part IV. Cobalt Carbides. *J. Phys. Soc. Jpn.* **1961**, *16*, 1213−1219.

(50) Ishida, K.; Nishizawa, T. The C-Co (carbon-cobalt) system. *J. Phase Equilib.* **1991**, *12*, 417−424.

(51) Meschel, S. V.; Kleppa, O. J. Standard enthalpies of formation of some 3d transition metal carbides by high temperature reaction calorimetry. *J. Alloys Compd.* **1997**, *257*, 227−233.

(52) Castner, D. G.; Watson, P. R.; Chan, I. Y. X-ray absorption spectroscopy, X-ray photoelectron spectroscopy, and analytical electron microscopy studies of cobalt catalysts. 2. Hydrogen reduction properties. *J. Phys. Chem.* **1990**, *94*, 819−828.

(53) Bulavchenko, O. A.; Cherepanova, S. V.; Malakhov, V. V.; Dovlitova, L. S.; Ishchenko, A. V.; Tsybulya, S. V. In situ XRD study of nanocrystalline cobalt oxide reduction. *Kinet. Catal.* **2009**, *50*, 192−198.

(54) Jacobs, G.; Ji, Y.; Davis, B. H.; Cronauer, D.; Kropf, A. J.; Marshall, C. L. Fischer−Tropsch synthesis: Temperature programmed EXAFS/XANES investigation of the influence of support type, cobalt loading, and noble metal promoter addition to the reduction behavior of cobalt oxide particles. *Appl. Catal., A* **2007**, *333*, 177−191.

(55) Ward, M. R.; Boyes, E. D.; Gai, P. L. In-situ Reduction of Co$_3$O$_4$ in H$_2$ using Environmental HRTEM. *J. Phys.: Conf. Ser.* **2014**, *522*, 012009.

(56) Karim, W.; Spreafico, C.; Kleibert, A.; Gobrecht, J.; VandeVondele, J.; Ekinci, Y.; van Bokhoven, J. A. Catalyst support effects on hydrogen spillover. *Nature* **2017**, *541*, 68.

(57) Werner, K.; Weng, X.; Calaza, F.; Sterrer, M.; Kropp, T.; Paier, J.; Sauer, J.; Wilde, M.; Fukutani, K.; Shaikhutdinov, S.; Freund, H.-J. Toward an Understanding of Selective Alkyne Hydrogenation on Ceria: On the Impact of O Vacancies on H2 Interaction with CeO$_2$(111). *J. Am. Chem. Soc.* **2017**, *139*, 17608−17616.

(58) Arnoldy, P.; Moulijn, J. A. Temperature-programmed reduction of CoOAl$_2$O$_3$ catalysts. *J. Catal.* **1985**, *93*, 38−54.

(59) Nagaoka, K.; Takanabe, K.; Aika, K.-i. Influence of the reduction temperature on catalytic activity of Co/TiO 2 (anatase-type) for high pressure dry reforming of methane. *Appl. Catal., A* **2003**, *255*, 13−21.

(60) Ruiz Puigdollers, A.; Schlexer, P.; Tosoni, S.; Pacchioni, G. Increasing Oxide Reducibility: The Role of Metal/Oxide Interfaces in the Formation of Oxygen Vacancies. *ACS Catal.* **2017**, *7*, 6493−6513.

(61) Özkara-Aydınoğlu, Ş.; Özensoy, E.; Aksoylu, A. E. The effect of impregnation strategy on methane dry reforming activity of Ce promoted Pt/ZrO$_2$. *Int. J. Hydrogen Energy* **2009**, *34*, 9711−9722.

(62) Wolfbeisser, A.; Sophiphun, O.; Bernardi, J.; Wittayakun, J.; Föttinger, K.; Rupprechter, G. Methane dry reforming over ceria-zirconia supported Ni catalysts. *Catal. Today* **2016**, *277*, 234−245.